Highlights on Spanish Astrophysics IX, Proceedings of the XII Scientific Meeting of the Spanish Astronomical Society held on July 18 – 22, 2016, in Bilbao, Spain. S. Arribas, A. Alonso-Herrero, F. Figueras, C. Hernández-Monteagudo, A. Sánchez-Lavega, S. Pérez-Hoyos (eds.)

Understanding the clumpy star-formation in local (U)LIRGs: A near-IR IFS perspective

Javier Piqueras López[1,2], Luis Colina[1], Santiago Arribas[1] Miguel Pereira-Santaella[1,2] Almudena Alonso-Herrero[1,3]

[1] Centro de Astrobiología (INTA-CSIC), Ctra de Torrejón a Ajalvir, km 4, 28850 Torrejón de Ardoz, Madrid, Spain
[2] Department of Physics, University of Oxford, Denys Wilkinson Building, Keble Road, Oxford OX1 3RH, UK
[3] Instituto de Física de Cantabria (CSIC-UC), Avenida de los Castros S/N, 39005 Santander, Spain

Abstract

The importance of Luminous and Ultraluminous Infrared Galaxies (U/LIRGs) in the context of the cosmological evolution of the star formation has been well established in the last decades. In particular, the study of local U/LIRGs using near-IR integral field spectroscopic techniques allows us to disentangle the 2D distribution of the star-formation using high spatial resolution, and characterise dust-enshrouded, spatially-resolved star-forming regions with great amount of detail. We present a comprehensive 2D IFS near-IR study of the extinction-corrected star-formation in a local sample of 10 LIRGs and 7 ULIRGs, based on VLT-SINFONI observations. We investigate the spatially-resolved distribution of the extinction-corrected star-formation rate (SFR) and star-formation rate surface density ($\Sigma_{\rm SFR}$) by analysing the Brγ and Paα emission of the galaxies of the sample. We also obtained integrated measurements of the SFR and $\Sigma_{\rm SFR}$, and identified a sample of 95 individual star-forming regions, characterised in terms of their size and Paα luminosity. These measurements will be discussed and compared with other SFR tracers like Hα, 24 μm and $L_{\rm IR}$, and other local and high-z samples of star-forming clumps.

1 Introduction

Star formation (SF) processes play a key role in our understanding of galaxy formation and evolution. These processes are governed by physical mechanisms that operate at very different scales, from mergers and gas flows to the pc scales of individual molecular clouds (see [6]). However, the coupling and hierarchy of the different mechanisms are not yet well understood.

In this context of the cosmological evolution of the SF, luminous (LIRGs, $10^{11}L_{\odot}<L_{\rm IR}<$

$10^{12}L_\odot$) and ultraluminous (ULIRGs, $10^{12}L_\odot < L_{IR} < 10^{13}L_\odot$) infrared galaxies play a central role (see e.g. [9], [8]). In particular, local U/LIRGs are valuable candidates for studying extreme cases of compact SF, coeval AGN, and their attendant feedback processes in a great amount of detail.

In this work, we present a detailed 2D near-IR IFS study of the extinction-corrected, global star formation rate (SFR), the sub-kpc structure of the star formation rate surface density (Σ_{SFR}), and the properties of individual star-forming clumps in a local sample of LIRGs and ULIRGs. For a more comprehensive analysis, see [12].

2 Sample and observations

The SINFONI sample comprises a representative set of 17 sources divided in two subsamples of 10 LIRGs and 7 ULIRGs, that cover the luminosity range of $\log(L_{IR}/L_\odot) = 11.10 - 12.43$. The mean redshifts of the LIRGs and ULIRGs subsets are $z_{LIRGs} = 0.014$ and $z_{ULIRGs} = 0.072$ and their mean luminosities are $\log(L_{IR}/L_\odot) = 11.33$ and $\log(L_{IR}/L_\odot) = 12.29$, respectively. For a detailed description of the sample, see [10].

The sample was observed with VLT-SINFONI, using the K-band 0.125" $\times$0.250" pixel^{-1} configuration of the instrument. The FoV of the resulting data cubes covers typically a size of $\sim 3 \times 3$ kpc for the LIRGs and $\sim 12 \times 12$ kpc for the ULIRGs subsample, with a resolution of ~ 0.63 arcsec (FWHM) that corresponds, on average, to ~ 0.2 kpc and ~ 0.9 kpc for LIRGs and ULIRGs. The average spectral resolution of the observations is R $\sim$ 3300.

As described in [10], the emission line maps were obtained by fitting a single Gaussian profile to the Paα and Brγ lines, after the data were binned using a Voronoi tessellation [4].

3 Data analysis

To study the star formation using our SINFONI data, we focused on the hydrogen recombination tracers that relate the intensity of a particular emission line with the SFR through the ionising photon rate. The young and most massive stars produce considerable amount of ionising photons that ionise the surrounding gas that, due to recombination processes, creates line emission cascades including the Balmer, Paschen and Brackett series (see [6]).

In particular, we used the well-known calibration from [5], $SFR\,[M_\odot yr^{-1}] = 7.9 \times 10^{-42} \times L_{H\alpha}\,[erg\,s^{-1}]$, that assumes a Salpeter IMF from 0.1 to 100 $M_\odot$ and solar abundances, and the star formation has to remain constant over ~ 6 Myr for it to be applicable. From this expression, taking the recombination factors Hα to Paα and Brγ (T= 10,000 K and $n_e = 10^4\,cm^{-3}$, case B) into account, we can directly obtain equivalent relations in terms of the Paα and Brγ luminosities.

The measurements of the SFR and Σ_{SFR} were derived using the Brγ and Paα emission lines for LIRGs and ULIRGs, respectively, and the calibrations presented above. These values were then corrected from extinction using A_V measurements from [11], obtained in terms of the Brγ/Brδ and Paα/Brγ line ratios, and the extinction law described in [3].

4 Star formation in local LIRGs and ULIRGs

4.1 Spatially resolved star formation on (sub)kiloparsec scales

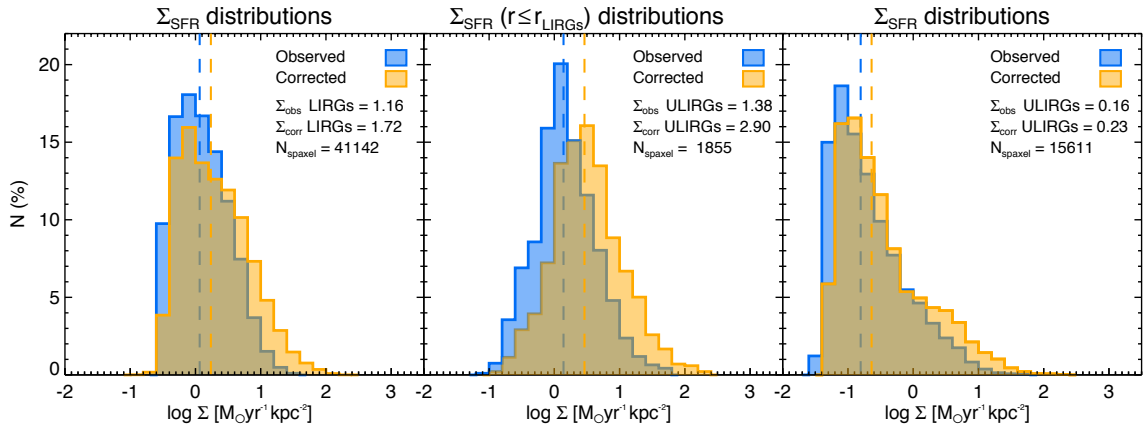

Figure 1: Observed and extinction-corrected spaxel-by-spaxel $\Sigma_{\rm SFR}$ distributions of the LIRG subsample (*left*), of the inner spaxels ($r \leq r_{\rm LIRGs}$, see text for details) of the ULIRG subsample (*centre*), and the complete ULIRG distributions (*right*). The median $\Sigma_{\rm SFR}$ values and the total number of spaxels in each distribution are shown in the panels in units of $[M_\odot\,yr^{-1}\,kpc^{-2}]$, and plotted as dashed vertical lines.

Figure 1 shows the observed and extinction-corrected $\Sigma_{\rm SFR}$ distributions for the sample of LIRGs and ULIRGs, resulting from combining all the individual spaxels from the individual $\Sigma_{\rm SFR}$ maps. In LIRGs, the median of the observed distribution is $\Sigma^{\rm obs}_{\rm LIRGs} = 1.16\,M_\odot\,yr^{-1}\,kpc^{-2}$, and increases to $\Sigma^{\rm corr}_{\rm LIRGs} = 1.72\,M_\odot\,yr^{-1}\,kpc^{-2}$ in the extinction-corrected distribution. In ULIRGs, the median values are $\Sigma^{\rm obs}_{\rm ULIRGs} = 0.16\,M_\odot\,yr^{-1}\,kpc^{-2}$ for the observed, and $\Sigma^{\rm corr}_{\rm ULIRGs} = 0.23\,M_\odot\,yr^{-1}\,kpc^{-2}$ for the extinction-corrected distribution, respectively.

The difference in distance, and hence in angular resolution between LIRGs and ULIRGs means that comparing their results is not straight-forward. The FoV of our SINFONI observations limits our analysis of the LIRGs to their innermost ~ 3 kpc with a typical sampling of about 200 pc. On the other hand, ULIRGs are located at larger distances, and the physical area covered by SINFONI FoV is about $\times 16$ that for LIRGs with a lower spatial resolution of about 0.9 kpc.

The central panel of Fig. 1 shows the resulting observed and extinction-corrected $\Sigma_{\rm SFR}$ distributions when comparing LIRGs and ULIRGs on the same physical regions, i.e. the innermost spaxels of the ULIRG distributions that corresponds to the same physical regions sampled in the LIRGs. We estimated an average radius, $r_{\rm LIRGs} = 1.4$ kpc, that correspond to the spaxel-weighted mean of the LIRG FoVs, and considered only those spaxels from the ULIRG distribution within this physical scales. When we consider only these values, the median extinction-corrected $\Sigma_{\rm SFR}$ values for LIRGs and ULIRGs are within a factor of 2.

4.2 Characterization of star-forming clumps

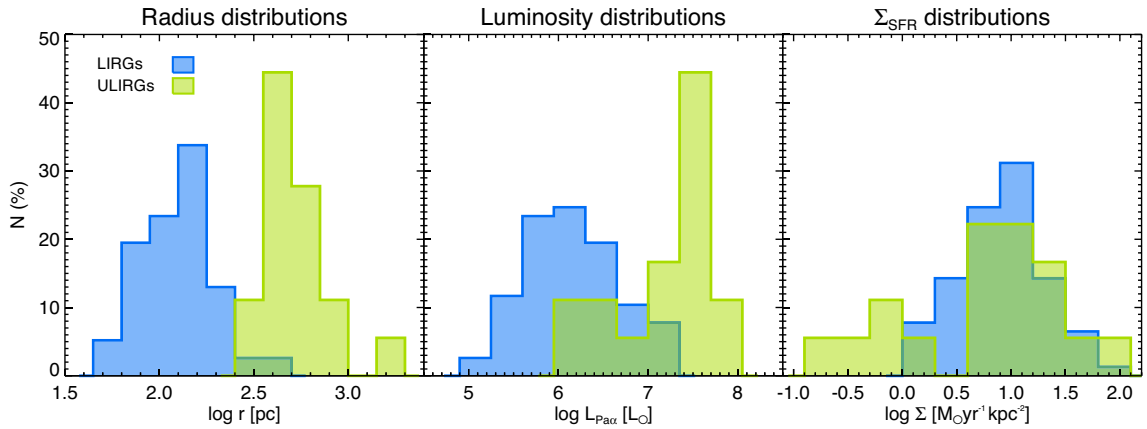

Figure 2: Distributions of the radius (*left*), extinction-corrected Paα luminosities (*centre*), and extinction-corrected $\Sigma_{\rm SFR}$ (*right*) of the star-forming regions from LIRGs (blue) and ULIRGs (green).

We have identified a total of 95 individual star-forming regions/complexes on the Brγ and Paα maps of LIRGs and ULIRGs, respectively. We derived their sizes, line luminosity and extinction-corrected $\Sigma_{\rm SFR}$ by fitting the light profile of the region using a 2D Gaussian function. Further details on the method and how it compares with other approaches like the half-light radius could be found in [12]. The distribution of the radius, $L_{Pa\alpha}$, and $\Sigma_{\rm SFR}$ is shown in Fig. 2. The star-forming regions have sizes in the ∼60 to 400 pc range for LIRGs and ∼300 to 1500 pc for ULIRGs, and extinction-corrected luminosities between $\sim 10^5$–$10^7\,L_\odot$ and $\sim 10^6$–$10^8\,L_\odot$ for LIRGs and ULIRGs, respectively, that yield $\Sigma_{\rm SFR}$ values of 1–90 $M_\odot\,yr^{-1}\,kpc^{-2}$ and 0.1–100 $M_\odot\,yr^{-1}\,kpc^{-2}$ for LIRG and ULIRG clumps. Given the average spatial resolution of our dataset, some of the smallest regions in the LIRG subsample, and some of the clumps in the ULIRG subset, are essentially unresolved.

4.3 Star-forming clumps in U/LIRGs: comparison with nearby and high-z galaxies

We compared our measurements with different samples of star-forming clumps in nearby galaxies. Although most of the data from other samples correspond to Hα measurements (e.g. [1]), we converted the extinction-corrected Hα luminosities into Paα luminosities using the case B recombination factor at T= 10,000 K and $n_e = 10^4\,cm^{-3}$ ($L_{H\alpha}/L_{Pa\alpha} = 8.582$). Details of these different datasets taken from the literature can be found in [12].

Figure 3 shows the Paα radius - luminosity relations of our sample of clumps, compared with nearby (*left*) and high-z star-forming regions (*right*). The blue line in Fig. 3 correspond to the power law fitting $L_{Pa\alpha} \sim r^\eta$ to the local points (i.e. U/LIRGs and local samples), that yields an exponent of $\eta = 3.04$. This value is in very good agreement with what it would be expected for photon-bounded regions, represented by Strömgren spheres. However,

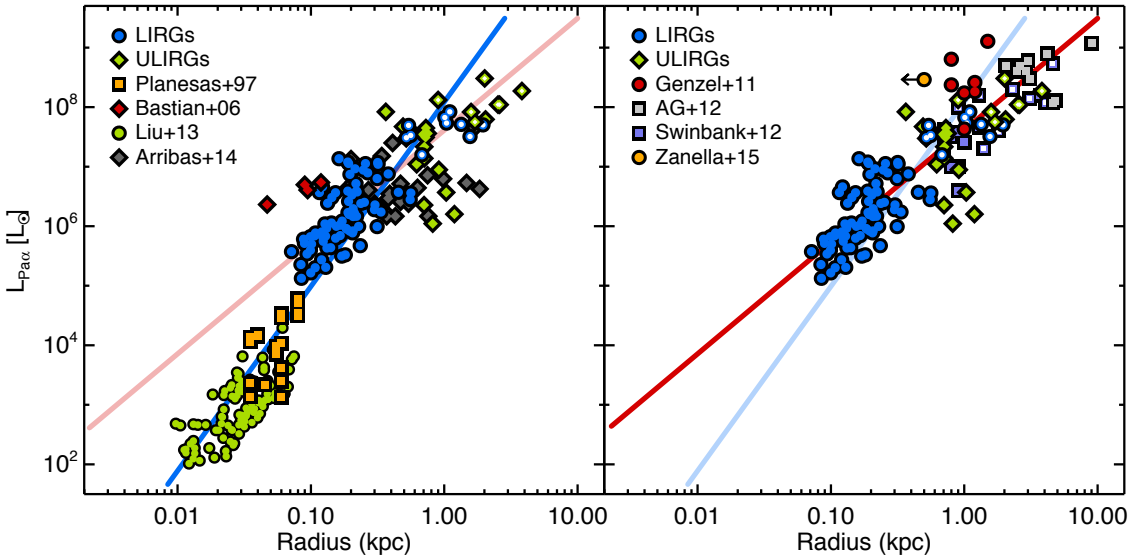

Figure 3: Extinction-corrected $L_{Pa\alpha}$ versus radius of individual star-forming clumps and galaxies. The individual regions of LIRGs and ULIRGs are plotted as blue circles and green diamonds, respectively, whereas the integrated measurements of each object of our sample are marked using hollow symbols. We show the comparison with local samples (*left*) and high-z samples (*right*). The blue and red lines correspond to power law fits $L_{Pa\alpha} \sim r^{\eta}$ to our data of local LIRG and ULIRG clumps, together with the local samples ($\eta = 3.04$) and high-z points ($\eta = 1.88$), respectively. See [12] for further details about the samples.

it seems to be a clear change on the slope at r$\sim$ 60 pc, that corresponds approximately to $L_{Pa\alpha} \sim 10^5\,L_\odot$. This value coincides with the proposed luminosity threshold from photon- to density-bounded regions by [2].

There are different physical and observational effects that could produce deviations from this model. If the regions are density-bounded, i.e. the hydrogen atoms recombine faster than they are ionised and some ionising photons scape, a shallower slope of the L-r is expected. On the other hand, other observational biases as region blending, low S/N ratio of the clumps or different spatial resolution of local and high-z observations might also contribute to change the slope of the L-r relation ([14], [7]).

We also compared our measurements with samples of high-z galaxies (Fig. 3, *right*). However, our dataset is not well suited to study and simulate the effect of distance at higher redshifts, given the limited FoV of our SINFONI observations. Therefore, we restricted the comparison at clump level only for those AO-based samples. When compared with high-z star-forming regions, clumps in LIRGs appear as significantly ($\sim$3-20 times) smaller than the kpc-size clumps detected so far at high-z, and up to 1000 times less luminous. On the other hand, clumps in ULIRGs have sizes similar ($\times$0.5–1) to that of high-z clumps, having Paα luminosities similar to some high-z clumps and about 10 times less luminous that the most luminous high-z clumps identified so far.

These results suggest that the giant clumps in high-z star-forming galaxies appear to be forming stars with a higher surface density rate than ULIRGs, and in particular LIRGs. This could be the consequence of a higher molecular gas surface density in the high-z sources, and therefore a higher SFR, as expected if the empirical Kennicutt-Schmidt law, valid on a galaxy scale, also applies at the (sub)kpc scales in the highly luminous and dense environments of U/LIRGs and/or high-z galaxies.

We found a slope for the L-r relation of the U/LIRGs and high-z clumps of $\eta \sim 1.88$. The large scatter in the Paα luminosity among the high-z clumps (Fig. 3, *right*) could indicate a similar break of the KS law at high-z. The sample of high-z clumps is however still very limited and consist of a few clumps in luminous (SFR $\sim 120 - 290\,\mathrm{M}_\odot\ \mathrm{yr}^{-1}$), and fainter (SFR $\sim 16\,\mathrm{M}_\odot\ \mathrm{yr}^{-1}$) extended star-forming disks. A proper comparison of low- and high-z luminous star-forming galaxies with larger samples is required to investigate more deeply the differences of the star formation on (sub)kpc scales. Planned future instrumentation, e.g. HARMONI [15] for the E-ELT will imply a huge step further in our understanding of star formation processes in these systems.

Acknowledgments

This work was supported by the Ministerio de Economía y Competitividad of Spain under the grant AYA2012-39408-C02-01, and by the Science and Technology Facilities Council (STFC) grant ST/N002717/1. We certainly acknowledge the Editors of Highlights of Spanish Astrophysics VII and VIII for their help while preparing this documentation.

References

[1] Arribas, S., Colina, L., Bellocchi, E., et al. 2014, A&A, 568, A14

[2] Beckman, J. E., Rozas, M., Zurita, A., et al. 2000, AJ, 119, 2728

[3] Calzetti, D., Armus, L., Bohlin, R. C., et al. 2000, ApJ, 533, 682

[4] Cappellari, M., & Copin, Y. 2003, MNRAS, 342, 345

[5] Kennicutt, R. C. J. 1998, ARA&A, 36, 189

[6] Kennicutt, Jr., R. C., & Evans, II, N. J. 2012, ARA&A, 50, 531

[7] Liu, G., Calzetti, D., Kennicutt, R. C. J., et al. 2013, ApJ, 772, 27

[8] Magnelli, B., Popesso, P., Berta, S., et al. 2013, A&A, 553, A132

[9] Pérez-González, P. G., Rieke, G. H., Egami, E., et al. 2005, ApJ, 630, 82

[10] Piqueras López, J., Colina, L., Arribas, S., et al. 2012, A&A, 546, A64

[11] Piqueras López, J., Colina, L., Arribas, S., et al. 2013, A&A, 553, A85

[12] Piqueras López, J., Colina, L., Arribas, S., et al. 2016, A&A, 590, A67

[13] Rieke, G. H., Alonso-Herrero, A., Weiner, B. J., et al. 2009, ApJ, 692, 556

[14] Scoville, N. Z., Polletta, M., Ewald, S., et al. 2001, AJ, 122, 3017

[15] Thatte, N. A., Clarke, F., Bryson, I., et al. 2016, Proc. of SPIE, Vol 9908, doi:10.1117/12.2230629